1 **Tundra uptake of atmospheric elemental mercury drives Arctic mercury**
2 **pollution**

3

4 **Authors:** Daniel Obrist[1,2*], Yannick Agnan[2,3], Martin Jiskra[4], Christine Hedge[2], Dominique
5 Colegrove[5], Jacques Hueber[5], Christopher Moore[2,6], Jeroen Sonke[4], Detlev Helmig[5]

6

7 **Affiliations:**

8 [1]Department of Environmental, Earth, and Atmospheric Sciences, University of Massachusetts,
9 Lowell, MA 01854, USA

10 [2]Division of Atmospheric Sciences, Desert Research Institute, 2215 Raggio Parkway, Reno,
11 Nevada 89512, USA.

12 [3]Milieux Environnementaux, Transferts et Interactions dans les hydrosystèmes et les Sols
13 (METIS), UMR 7619, Sorbonne Universités UPMC-CNRS-EPHE, 4 place Jussieu, F-75252 Paris,
14 France.

15 [4]Geosciences Environnement Toulouse, CNRS/OMP/Université de Toulouse, 14 Avenue Edouard
16 Belin, 31400 Toulouse, France.

17 [5]Institute of Arctic and Alpine Research (INSTAAR), University of Colorado, 4001 Discovery
18 Drive, Boulder, Colorado 80309, USA.

19 [6]Gas Technology Institute (GTI), 1700 S Mount Prospect Road, Des Plaines, Illinois 60018, USA.

20

21

22 *Corresponding Author: E-mail: Daniel_obrist@uml.edu

23

24

25   **Anthropogenic activities have led to largescale mercury (Hg) contamination in the Arctic[1-3]**

26   **so that Hg tissue levels in modern-day wildlife including falcon and eagle feathers, polar bear**

27   **hairs, and beluga whale teeth, are enhanced up to 10-fold[4-6]. High Arctic Hg contamination**

28   **has been attributed to unique sea-salt-induced chemical cycling of Hg, termed Atmospheric**

29   **Mercury Depletion Events (AMDEs), but their impacts are now debated[2,7] and are largely**

30   **unknown away from the coast. Furthermore, wet deposition measurements in the Arctic**

31   **show some of the lowest Hg deposition via precipitation worldwide[8] raising questions as to**

32   **the sources of high Arctic Hg exposure. Based on the most comprehensive Hg deposition**

33   **mass balance study so far, here we show that the main source of Hg (71%) in the interior**

34   **Arctic tundra is derived from gaseous elemental Hg (Hg^0) deposition, rather than deposition**

35   **via precipitation or AMDEs – which are both minor. Deposition of Hg^0, the form**

36   **ubiquitously present in the global atmosphere, occurs throughout the year, including the**

37   **Arctic winter, and is enhanced in summer by vegetation Hg^0 uptake. The tundra uptake of**

38   **gaseous Hg^0 leads to high soil Hg concentrations and mass exceeding levels in temperate soils**

39   **several-fold. Concurrent Hg stable isotope measurements in the atmosphere, snowpack,**

40   **vegetation, and soils support that Hg^0 dominates as a source to the tundra, and we hence for**

41   **the first time provide a fully independent confirmation of Hg isotope source tracing. Stable**

42   **isotope data from an inland to coastal transect show high soil Hg consistently derived from**

43   **Hg^0, suggesting that the Arctic tundra forms a globally-important Hg sink storing up to half**

44   **the world's soil Hg. High tundra soil Hg also explains why rivers annually transport massive**

45   **amounts of Hg (50–80 Mg y^{-1}) to the Arctic Ocean[9-11]. Hg stable isotope signatures now also**

46   **suggest that Hg^0 may dominate as sources in mid-latitude ecosystems[12-15], and we hence call**

47   **for a focus on monitoring strategies for Hg^0 deposition worldwide.**

48   Hg pollution impacts are increasingly controlled by climate-change induced disturbances in

49   aquatic and terrestrial biogeochemistry[16], with potentially the most significant consequences in the

50   Arctic where warming occurs at a rate almost double the worldwide average[17,18]. Regulatory

51   frameworks such as the recent UNEP Minamata Convention – aimed to reduce Hg contamination

52   globally[19] – rely on understanding of Hg sources, which is currently lacking in the Arctic. The

53   widespread Hg contamination observed across the Arctic is inconsistent with extremely low

54   atmospheric wet deposition, which in Arctic ecosystems is found to be among the lowest globally.

55   For example, annual wet deposition of 2.1±0.7 µg m^{-2} yr^{-1} at Gates of the Arctic National Park in

56   Alaska (Supplemental Table S1) is almost five times lower than wet deposition measured across

57   99 lower-latitude U.S. locations (9.7±3.9 µg m^{-2} yr^{-1})[8]. Also unclear are the origins of vast amounts

58   of Hg that are annually transferred by Arctic rivers to the Arctic Ocean[9]. These riverine Hg inputs

59   to the Arctic Ocean, which exceed direct atmospheric deposition[10,11], stand in contrast to

60   predictions that rank Arctic catchments lowest in terms of watershed Hg storage globally[20].

61   Another potential Hg source, deposition due to sea-salt-induced AMDEs in springtime[21], long was

62   thought to be responsible for high Arctic Hg deposition. However, AMDEs may cause much

63   smaller net Hg deposition because most of the deposited Hg can revolatilize to the atmosphere

64   before snow melts and studies provide inconclusive evidence about their importance for Arctic

65   deposition[2,7].

66   Unlike wet deposition and deposition related to AMDEs, both of which are composed of oxidized

67   Hg (Hg^{II}), deposition of gaseous elemental Hg^0 – the form which is subject to long-range

68   atmospheric transport and global atmospheric distribution – is largely unconstrained and not

69   measured by deposition networks. We recently reviewed 132 studies on gaseous Hg^0 exchange

70   between the atmosphere and terrestrial surfaces and estimated net global terrestrial Hg^0 exchange

71   to exhibit a wide range and large uncertainty, from a net deposition of 500 Mg yr^{-1} to a net emission

72   (i.e., volatilization from ecosystems to the atmosphere) of 1650 Mg yr^{-1} [22]. The large uncertainty

73   stems from an almost complete lack of whole-ecosystem Hg^0 exchange measurements among

74   these studies.

75   Here we performed a mass balance of atmospheric Hg deposition in the Arctic tundra – a biome

76   covering ~6% of the global land surface area – to determine the major Hg sources in one of the

77   most remote ecosystems worldwide. We conducted a two-year field measurement campaign to

78   constrain atmospheric Hg deposition at Toolik Field station on the North Slope of Alaska, USA,

79   200 km inland from the coast representing the interior tundra. We measured net gaseous Hg^0

80   exchange at the ecosystem-level using micrometeorological techniques, wet and dry Hg^{II}

81   deposition, and vegetation Hg inputs from aboveground biomass. We correspondingly measured

82   Hg stable isotopic signatures in the atmosphere, snowpack, vegetation, and soil, and quantified

83   total mass of Hg sequestered in tundra snowpack, plants, and soils. We further measured

84   atmosphere-snow-soil Hg^0 gas concentration profiles to independently verify Hg^0 flux exchange

85   and locate zones of atmospheric Hg^0 sources and sinks.

86   Gaseous Hg^0 was the dominant form of deposition (6.5 ± 0.7 µg m^{-2} yr^{-1}) accounting for 71% of

87   total deposition (Fig. 1). Wet Hg^{II} deposition amounted to less than 5% of Hg^0 deposition

88   (Supplemental Table S2; 0.2 ± 0.1 µg m^{-2} yr^{-1}) and even lower than previous low measurements

89   from another Arctic site in Alaska[8]. Atmospheric Hg^{II} concentrations were below the detection

90   limit (33 pg m^{-3}) during most of the measured period with the exception of March and early April

91   during AMDEs when concentrations reached nearly 0.5 ng m^{-3} (Extended Data). We constrained

92   atmospheric Hg^{II} dry deposition to 2.5 µg m^{-2} yr^{-1} (range 0.8 to 2.8 µg m^{-2} yr^{-1}) based on periodic

93   measurements of atmospheric Hg^{II} concentrations (Supplemental Information). We observed

94   temporarily elevated snow Hg levels during AMDEs, although the deposited Hg revolatilized to

95   the atmosphere within days (Supplementary Information).

96   The dominance of gaseous Hg^0 deposition as a source to this ecosystem was independently

97   confirmed by Hg stable isotope analyses. We comprehensively characterized Hg stable isotope

98   composition of atmospheric Hg^0, snowfall and snowpack, vegetation, organic and mineral soil

99   horizons, and bedrock samples. As observed in previous studies[12-15,23,24], atmospheric Hg^0 and

100   Hg^{II}, bedrock Hg^{II}, and Hg^{II} deposited through AMDEs have unique $\delta^{202}Hg$, $\Delta^{199}Hg$, and $\Delta^{200}Hg$

101   signatures (Fig. 2 and Extended Data). We then quantified relative contributions of different Hg

102   sources to vegetation and soil samples using endmember mixing models and triple isotopic

103   signatures. Results show that atmospheric gaseous Hg^0 is the dominant source of Hg in vegetation

104   (median: 90%), organic soils (73%), and upper mineral soils (55%). Hg^{II} deposition accounted for

105   10% to 22% of Hg in the two soil compartments; and residual Hg^{II} from AMDEs, transferred to

106   the tundra soils after snowmelt, accounted for 0–5%. Geogenic Hg contributed in a range of 0%

107   in organic soil horizons to ~40% in mineral soil horizons. These results confirm direct flux

108   measurements demonstrating that gaseous Hg^0 deposition is the dominant source of mercury to the

109   tundra at Toolik Field station. We measured soil Hg stable isotope signatures in three additional

110   tundra sites along a transect from Toolik Field station to the Arctic Ocean (Fig. 2D) and considered

111   values from an additional peat profile from Barrow, AK at the coast[24], and found no significant

112   differences in isotope signatures between these soils and soils at Toolik Field station. We hence

113   observed no higher contributions of AMDEs (maximum 5%) even in soils closer to the coast, and

114   show evidence that the source of Hg in tundra soils is consistently and predominantly derived from

115   atmospheric Hg^0 uptake.

116   Continuous flux measurements allowed determination of temporal patterns of Hg^0 deposition.

117   Gaseous Hg^0 deposition persisted throughout periods of snow cover (Fig. 1), with the exception of

118   March and April when net emission of Hg^0 to the atmosphere was observed after AMDEs. From

119   October through mid-May, Hg^0 deposition averaged 0.4 ± 0.4 ng m^{-2} h^{-1} and accounted for 37% of

120   total annual Hg^0 deposition. Gaseous Hg^0 concentration profiles in snow and soil air, measured

121   with complementary trace gas systems (see Methods), confirmed that wintertime Hg^0 deposition

122   occurred (Fig. 3). Snow pore air Hg^0 concentrations were consistently below atmospheric

123   concentrations, and concentrations decreased further from the upper to lower snowpack such that

124   concentrations at the soil-snow interface were less than 50% of atmospheric levels. Since diffusive

125   and advective trace gas fluxes are a function of respective concentration gradients, these Hg^0

126   concentration profiles were consistent with a net atmospheric deposition flux of gaseous Hg^0 to

127   the tundra ecosystem, providing a third means of verifying atmospheric Hg^0 deposition. Further

128   analysis showed that the wintertime Hg^0 deposition was driven by a sink below the Arctic

129   snowpack, most likely in the tundra soil (Supplementary Information). Such a soil Hg^0 sink has

130   been observed in a temperate soil, but the mechanism for soil Hg^0 uptake remains unclear[25].

131   During snow-free periods from mid-May through September, Hg^0 deposition increased (rate of

132   1.4 ± 1.0 ng m^{-2} h^{-1}) and continued to greatly exceed deposition of all other forms of Hg combined

133   (78% of total summertime deposition). In fact, some of the strongest Hg^0 deposition occurred after

134   the spring onset of the tundra vegetation growing season, indicating that tundra vegetation

135   amplified gaseous Hg^0 deposition. Clearly identifiable by its Hg isotope signature (Fig. 2), Hg in

136   aboveground vegetation was indeed primarily (90%) derived from atmospheric Hg^0 uptake as

137   shown previously[12,14]. We calculated substantial Hg mass contained in aboveground vegetation

138   (29 µg m^{-2}; Table S4) which can subsequently be transferred to tundra soils via plant senescence

139   and litterfall.

140   The dominant and time-extended atmospheric deposition of gaseous Hg^0 to the Arctic tundra has

141   implications for local, regional, and global Hg cycling. Deposition of globally ubiquitous gaseous

142   Hg^0 leads to unexpectedly high Hg levels in these remote tundra soils. Based on ^{14}C age dating

143   that shows that soils at Toolik Field station are older than 7,300 years (Table S5), deposition of

144   atmospheric Hg^0 and accumulation of Hg in soils must have occurred over millennia. Soil Hg

145   concentrations in the active layer above the permafrost averaged 138±15 µg kg^{-1} in organic soil

146   layers and 97±13 µg kg^{-1} in mineral soil horizons (Table S5), exceeding the 20–50 µg kg^{-1} range

147   observed across temperate and tropical soils several-fold[26-28]. Riverine studies suggest that

148   significant contributions by upland soil sources in the Arctic are needed in order to explain high

149   Hg loadings[9,10]. The high tundra soil Hg levels, derived from Hg^0 uptake, hence explain the

150   conundrum that watersheds with some of the lowest Hg wet deposition loads on Earth and limited

151   impacts from AMDEs show elevated Hg in rivers and widespread Hg impacts on Arctic wildlife[3-

152   6].

153   At the global scale, the Arctic tundra serves as an important repository for atmospheric Hg^0 emitted

154   at mid-latitudes. Stable isotope analysis across four different tundra soils on the North Slope of

155   Alaska confirm that atmospheric Hg^0 dominates as a source and suggests a large-scale Hg^0 sink

156   across the Arctic tundra. Although few soil tundra Hg concentrations are reported elsewhere, our

157   measurements along a 200 km northern Alaska transect and a few published data also show high

158   soil Hg concentrations (Table S6). If a soil Hg pool of 27 mg m^{-2} at Toolik Field station (Table S5;

159   top 40 cm) is representative of the global tundra belt, Arctic tundra soils would contain ~143 Gg

160   of Hg, which would account for almost half the total estimated global soil Hg pool size of 300 Gg

161   based on temperate studies for this soil depth[20,29]. Further, our study provides the first independent

162   experimental verification of source attribution by Hg isotope signatures, which at this tundra site

163   show that Hg stored in vegetation and soils is predominantly derived from atmospheric Hg^0

164   consistent with direct deposition measurements. Recent Hg stable isotope studies have suggested

165   that gaseous Hg^0 deposition may dominate as a source in remote forests of the mid-latitudes[12-15]

166   as well. We hence call upon regulators and the scientific community to reorganize deposition

167   monitoring[30] to include deposition of Hg^0 which we expect to dominate as a source across remote

168   ecosystems worldwide.

169

170 **Methods:**

171 ***The study site*** is located near Toolik Field station (68°38'N, 149°36'W), a research station

172 operated by the University of Alaska, Fairbanks. All measurement systems were located in a

173 tussock tundra with underlying soil types characterized as Typic Aquiturbels with active layer

174 depths between 60 and 100 cm. All analyzers and control systems were housed in a temperature-

175 controlled field laboratory (Extended Data Fig. E1) built on the tundra, and sampling lines and

176 sensors were routed outside to the tundra sampling locations via heated conduits. This setup

177 allowed year-round measurements of trace gas dynamics including through the Arctic winter

178 without damage from icing, animal disturbances, or other issues.

179 ***Overview of key measurements:*** During two full years, we measured continuous net surface-

180 atmosphere fluxes of gaseous Hg^0 (i.e., the balance of deposition and volatilization), that to our

181 knowledge was conducted year-round previously only in two temperate grassland sites[31,32].

182 Campaign-style wet deposition measurements composed of Hg^{II} species[33] were conducted

183 approximately every six weeks throughout the two years and included snowfall and rain

184 measurements, surface snow and full snowpack collection, and subsequent analysis of total

185 dissolved Hg after melting. Hg^{II} dry deposition was assessed by pyrolyzer measurements (see

186 below) to quantify atmospheric Hg^{II} concentrations multiplied by deposition velocity. Hg^{II} dry

187 deposition measurements were conducted only from January through September 2016, but we used

188 auxiliary Arctic studies to constrain mid-winter patterns[1, 34] (see below and Extended Data). In

189 addition, we measured gaseous Hg^0 in interstitial air of snowpack and tundra soils at multiple

190 locations and depths in the tundra during two full years to assess atmosphere-snow-soil diffusion

191 profiles and pinpoint active source and sink zones. For this, a snow tower (Fig. E1D;[35,36]) was

192 deployed to measure Hg^0 gas concentrations in interstitial snow pores at multiple depths in the

193 undisturbed tundra snowpack. In addition, a soil trace-gas system (Fig. E1E[37]) consisting of six

194 gas wells provided gaseous Hg^0 concentrations in soil pores at three depths each in two tundra soil

195 profiles. During summers, field campaigns were conducted for detailed characterization of

196 concentrations and pool sizes of Hg in all major ecosystem matrices, including vegetation as well

197 as organic and mineral soil layers. Characterization of Hg stable isotope compositions were

198 conducted in snow, soils, plants, and the atmosphere to complement source and sink processes of

199 Hg in this tundra ecosystem.

200   ***Micrometeorological flux measurements*** to quantify gaseous Hg^0 exchange at the ecosystem level

201   were conducted using an aerodynamic flux method (Fig. E1C). Surface-atmosphere flux was

202   calculated by measurement of concentration gradients in the atmosphere above the tundra in

203   conjunction with atmospheric turbulence parameters as follows:

204   $$F_{Hg^0} = -\frac{k * u_* * z}{\phi_h(z/L)} * \frac{\partial c(Hg^0)}{\partial z} \quad (1)$$

205   where k denotes the von Karman constant (0.4), u_* the friction velocity, z the measurement height,

206   $\phi_h(z/L)$ the universal temperature profile, L the Monin-Obukhov length, and $\partial c(Hg^0)/\partial z$ the

207   vertical Hg^0 gas concentration gradient. Hg^0 concentrations at heights of 61 cm and 363 cm above

208   the soil surface were measured through 0.2 μm Teflon® inlet filters connected to perfluoroalkoxy

209   (PFA) lines, a setup that measures gaseous Hg^0 [37]. A valve control system with three-way solenoid

210   valves (NResearch, West Caldwell, NJ, USA) allowed switching between the gradient inlets every

211   10 min. Solenoids were connected to a set of trace gas analyzers with a total sampling flow of 1.5

212   L min^{-1}. This system included an air mercury analyzer (Model 2537A, Tekran Inc. Toronto,

213   Canada); a Cavity Ring-Down (CRD) greenhouse gas analyzer to measure CO_2, H_2O, and CH_4

214   (Los Gatos Research, San Jose, USA); an O_3 analyzer (Model 49C, Thermo Scientific, Waltham,

215   USA); and an O_2 analyzer (Model 1440, Servomex, East Sussex, United Kingdom).

216   Fluxes were calculated only during periods of appropriate turbulence according to Edwards et al.[38]

217   and periods when $z/L < -0.2$ and $z/L > 0.2$ were removed from the data set. The tundra measurement

218   site was bordered by Toolik Lake to the north, and we removed data when flux footprints

219   originated from Toolik Lake or it's edge (0-40° and 300-360°, 27% of the data). For gap filling of

220   periods when measurements were missing, or when fluxes originated from the nearby lake, or

221   when conditions did not fulfill the criteria for acceptable turbulence to calculate fluxes, we

222   interpolated flux data using the average diel pattern of each respective month. For quality control,

223   sampling lines were confirmed to be free of contamination during each field visit (approximately

224   every six weeks using Hg-free air; Model 1100, Tekran Inc.). In addition, line inter-comparisons

225   were conducted at the same interval to test for line biases between the upper and lower inlet lines;

226   for this, both upper and lower inlet lines were set at the same height and measurements were

227   conducted to assess offset. Line intercomparison tests showed no significant line offsets

228   throughout the study with the exception of one time when a leak was detected and immediately

229   fixed, and fluxes prior to that time were corrected.

230   *A snow tower* (Fig. E1D) to measure gaseous Hg^0 and auxiliary trace gas concentrations in the

231   undisturbed snowpack at multiple heights was deployed next to the flux tower (approximately 2

232   m distant). The snow tower, described in Seok et al.[35] and Faïn et al.[36], consists of vertical square

233   aluminum bars with 60 cm cross arms at five heights that hold a total of 10 sampling inlets.

234   Horizontal crossbars that support air inlets were set at heights of 0, 10, 20, 30, and 110 cm above

235   the soil surface, with the lower four inlets generally buried in snow most of winter to measure

236   snow pore air; the uppermost inlet always was located above the snowpack and measured

237   atmospheric Hg^0 gas concentrations. Each crossbar supported a pair of connected air inlets, spaced

238   60 cm apart, and fitted with 25 mm syringe filters with 1 μm glass fiber membranes (Pall Life

239   Sciences, Ann Arbor, Michigan, USA) connected to PFA lines. Snow tower lines were connected

240   to a Teflon valve control box and data acquisition system inside the heated laboratory. These lines

241   were connected to a second set of trace gas analyzers, including for gaseous Hg^0, ozone (same

242   models as above), as well as a CO_2 and H_2O analyzer (Model LI840A, LI-COR Inc., Lincoln,

243   USA). Sampling flow rates were set between 2.7 and 3.0 L min^{-1}, and the sampling sequence was

244   set to extract snow air at each height for 10-min measurement periods so that a full sequence of all

245   five inlet heights was sampled every 50 min. Measurements of ambient air gaseous Hg^0

246   concentrations measured at the top inlet of the snow tower system compared well to ambient air

247   Hg^0 concentrations measured by the micrometeorological tower.

248   *A soil trace gas measurement system* (Fig. E1E), similar to a system described in Obrist et al.[25],

249   was deployed to allow monitoring of soil pore trace gases at multiple depths and locations. In the

250   first year, the soil trace gas system consisted of six Teflon wells (63.5 cm length, 10.2 cm diameter)

251   with inside volumes of 4.2 L. One side of each well was perforated with 65 holes of 0.64 cm

252   diameter for a total perforated area of 20.6 cm^2. The holes were covered with Gore-Tex®

253   membranes and Teflon screens, both of which were held in place by stainless steel brackets and

254   pipe clamps for a watertight seal, allowing gas diffusion into the wells while keeping out soil water.

255   The soil wells were placed at two tundra soil profiles (10 cm, 20 cm, and 40 cm depths); one profile

256   consisted mainly of organic soil layers and a second mainly of mineral horizons. The six wells

257   were connected by PFA lines to the heated laboratory and connected to the same set of

258   instrumentation to measure trace gas gradients for flux measurements (gaseous Hg^0, CO_2, H_2O,

259   CH_4, O_3, and O_2). The system, operated at a flow rate of 1.5 l min^{-1}, was programmed to extract a

260   sequence of soil measurements (10 min. each) only three times per day to reduce the air volume

261   extracted from the soil profile and minimize disturbance and advection effects. Because of water

262   intrusion into the soil gas wells in June 2015, the system was replaced with a different system

263   consisting of 47 mm Teflon inlet filters with additional inlet holes drilled at the bottom of the

264   filters and mounted upside down in the soil profile at the same six locations. Testing in saturated

265   water showed that the hydrophobic Teflon filters prevented water intrusion into the sampling lines

266   using this inlet configuration. Both soil trace gas systems were extensively tested in Hg-free air

267   and ambient air prior to deployment to confirm that they were free of contamination. These systems

268   showed quick equilibrium with ambient air Hg^0 concentrations, and there was no memory effect

269   when switching the sampling lines. Both measurement systems provided the same magnitude and

270   seasonal patterns of gaseous Hg^0 soil concentrations (Fig. 3).

271   ***Atmospheric Hg^{II} concentrations*** were measured using a third gaseous mercury analyzer (Model

272   2537; Tekran Inc.) in conjunction with a pyrolyzer unit. Hg^{II} concentrations were calculated by

273   differential measurements of air drawn from an inlet configured to measure gaseous Hg^0 (using

274   0.2 μm Teflon inlet filters) and a second inlet stream without a filter routed through a pyrolyzer

275   oven set at 650º C, whereby all atmospheric Hg forms were converted into gaseous Hg^0 (i.e.,

276   measure total Hg). A valve switching unit (Model 1110, Tekran Inc.) was used to alternate

277   measurements between total Hg and gaseous Hg^0 measurements every 10 min, and allowed

278   calculating Hg^{II} concentrations by difference (similar to Lyman and Jaffe[39]). As a pyrolyzer oven,

279   we modified a particulate mercury speciation module (Model 1135; Tekran Inc., Toronto, Canada)

280   and used a quartz tube filled with quartz chips as pyrolyzer inlet that directly reached the ambient

281   atmosphere for sampling. In addition, the particulate filter inside the glassware was removed, and

282   the quartz tube was filled with quartz chips to increase the surface area and serve as an efficient

283   catalyst. The detection limit of this system, based on three times standard deviation of the blanks,

284   was 33 pg m^{-3}. The pyrolyzer unit was deployed from January through September 2016.

285   Atmospheric Hg^{II} concentration measurements were lacking from October through mid-February,

286   but we found undetectable (<0.033 ng m^{-3}) or low concentrations (generally <0.05 ng m^{-3}) in other

287   winter months, similar to low or undetectable Hg^{II} concentrations outside of periods of AMDEs at

288   other Arctic locations[34]. For 2015, we assumed similar Hg^{II} concentrations as measured in 2016.

289   Negative numbers in the Hg^{II} record represent noise levels of differential measurements as well as

290   data are produced during strong fluctuations of total atmospheric Hg concentrations (i.e., during

291   AMDE depletion recoveries). Atmospheric deposition of Hg^{II} was calculated to be 2.5 µg m^{-2} yr^{-1}

292   based on multiplication of measured Hg^{II} concentrations with a proposed deposition velocity for

293   Hg^{II} of 1.5 cm s^{-1} over various surfaces[40], with a range from 0.8 to 2.8 µg m^{-2} yr^{-1} (based on

294   deposition velocities generally between 0.5 and 1.7 cm s^{-1})[41]. Even lower annual atmospheric Hg^{II}

295   deposition has been independently estimated for this area based on nearby Arctic lake studies (0.1

296   µg m^{-2})[1]. Low wintertime Hg^{II} concentrations and deposition are further consistent with extremely

297   low wintertime snowfall Hg concentrations (on average 0.26 ng L^{-1}; Supplementary Information

298   Table S2) – which are derived from Hg^{II} scavenged from the atmosphere. Finally, stable Hg

299   isotopic signatures were consistent with low amounts of Hg^{II} deposition measured at this site.

300   ***Atmospheric wet deposition of Hg (mainly Hg^{II} forms) and snow Hg^{II}*** was characterized by

301   frequent collection of surface snow and manual collection of rainfall using trace-metal collection

302   techniques (gloves, acid-cleaned Teflon and stainless steel sampling equipment). Samples were

303   analyzed for Hg concentrations after filtration with 0.45 µm pore size filters. A total of 19 sampling

304   dates were used for calculation of wet deposition loads (Table S2). Surface snow samples (top 3

305   cm) were directly transferred into new, sterile polyethylene sampling bags (Whirl-Pak®; Nasco,

306   Fort Atkinson, WI, USA). Fresh snow was directly taken from the surface into the sampling bags;

307   additional snowpack sampling was performed from the top to the bottom of the snowpack using

308   acid-cleaned stainless steel cutters (Model RIP 1 1000 cc cutter; Snowmetrics, Fort Collins, CO,

309   USA). In addition, snowpack sampling was performed on five dates using two excavated snow

310   pits each that were sampled using stainless steel snow cutter (RIP 1 cutter 1000 cc) and then

311   directly transferred to the sterile polyethylene sampling bags (double bags). Each snow pit was

312   sampled at 10 cm-layer increments from the top to the bottom of the snow pit. Per layer, two

313   replicate samples from perpendicular walls of the pit were each pooled together for analysis.

314   Summertime collection of rainwater was performed manually using an acid-cleaned Teflon funnel

315   and Teflon bottles. Determination of total dissolved Hg was performed according to U.S. EPA

316   Method 1631 for total mercury in water using dual stage gold pre-concentration and an Hg water

317   analyzer (Model 2600; Tekran Inc., Toronto, Canada). Annual atmospheric wet deposition was

318 calculated using volumetric precipitation measured at Toolik Field Station multiplied by respective

319 snow and rain Hg concentrations (Table S2). Hg_{tot} and Hg_{diss} concentrations were determined using

320 Tekran 2600 cold-vapor atomic fluorescence spectrometry (Tekran Instruments Corporation,

321 Toronto, ON, Canada) using a bromine monochloride (BrCl) and hydroxylamine hydrochloride

322 digestion following the EPA method 1631. The detection limits, determined as 3-times the

323 standard deviation of blank samples, averaged 0.08 ng L^{-1}. Recoveries as determined by 5 ng L^{-1}

324 standards analyzed after every 10 samples averaged between 93 and 107%. Laboratory and field

325 blanks were conducted both for the stainless-stell cutter (using water rinses) and the whirl-pak

326 bags used for snow sampling, and both showed no metal contamination (all blank determinations

327 below detection limits).

328 ***Soil and vegetation Hg concentrations*** were determined from samples collected during multiple

329 field sampling campaigns in spring through fall 2014, 2015, and 2016. All samples were freeze-

330 dried, milled, and analyzed according to U.S. EPA method 7473 using a total mercury analyzer

331 (Model MA-2000; Nippon Inc., Takatsuki, Japan) and as described in detail in Obrist et al.[26]. To

332 estimate annual Hg uptake by vegetation and standing aboveground biomass pools (Table S4),

333 data on vegetation dynamics (aboveground net primary productivity: NPP; and aboveground

334 vegetation biomass) were used from Shaver and Chapin[41] and Chapin et al.[42].

335 ***Hg Stable isotope measurements*** were performed on Hg extracted from subsamples of dried and

336 milled vegetation, soil, and rock samples using a two-step oven combustion system[14]. Snow

337 samples were processed using a purge and trap system described by Sherman et al.[23] which was

338 scaled up to 20 L bottles to attain Hg amounts large enough from low-concentrated snow samples.

339 Sample blanks, recoveries, and Hg isotopic composition of processing standards (NIST-3133)

340 were analyzed (Table E4). Atmospheric gaseous Hg^0 was collected continuously from a separate

341 inlet at the flux tower, equipped with a glass fiber filter (as described for snow tower

342 measurements) and a heated PFA line to the field laboratory. Atmospheric gaseous Hg^0 (typically

343 sampled at 0.2 lpm for periods of 6–8 weeks) was collected on iodated activated carbon traps (IC-

344 traps, 125 mg) which were processed with a combustion method adapted from Fu et al.[43]. Gaseous

345 Hg^0 breakthrough of IC-traps was measured regularly during the sampling campaign using a

346 Tekran 2537 mercury analyzer and was always below the detection limit (0.05 ng m^{-3}). Procedural

347 blanks, procedural standards, and sample recoveries were measured for quality assurance (Table

348   E1). Hg isotopic ratios were measured by cold vapor – multi-collector inductively coupled plasma

349   mass spectrometry (CV-MC-ICPMS; Neptune, Thermo-Finnigan, Germany) at the Midi-Pyrenees

350   Observatory (Toulouse, France) applying measurement protocols described elsewhere[13,43].

351   Hg isotopic signatures are expressed using common nomenclature of small delta notation for mass-

352   dependent signatures (MDF):

353   $$\delta^{xxx}Hg_{NIST-3133} = \left(\frac{(^{xxx}Hg/^{198}Hg)_{Sample}}{(^{xxx}Hg/^{198}Hg)_{NIST-3133}} - 1 \right) \times 10^3 \qquad (2)$$

354   where xxx corresponds to masses 199, 200, 201, 202, and 204. Mass-independent Hg isotopic

355   signatures (MIF) are expressed by capital delta notation:

356

357   $$\Delta^{yyy}Hg = \delta^{yyy}Hg - (\delta^{202}Hg \times sf) \qquad (3)$$

358   where yyy corresponds to the mass of 199, 200, 201, and 204 and *sf* to the kinetic mass-dependent

359   scaling factors of 0.2520, 0.5024, 0.7520, and 1.493 for $\Delta^{199}Hg$, $\Delta^{200}Hg$, $\Delta^{201}Hg$, and $\Delta^{204}Hg$,

360   respectively. Analytical precision and accuracy were assured through repetitive measurements of

361   in-house standards ETH-Fluka ($\delta^{202}Hg$ = -1.43±0.19‰, $\Delta^{199}Hg$ 0.08±0.07‰, $\Delta^{200}Hg$ 0.02±0.07‰,

362   2SD, n=38) and UM-Almaden ($\delta^{202}Hg$ = -0.56±0.10‰, $\Delta^{199}Hg$ -0.02±0.06‰, $\Delta^{200}Hg$

363   0.01±0.07‰, 2SD, n=9) which were in agreement with previously reported values[12-14].

References:

365   1.   Fitzgerald, W. F. *et al.* Modern and historic atmospheric mercury fluxes in northern Alaska: global
366   sources and Arctic depletion. *Environ. Sci. Technol.* **39**, 557-568 (2005).
367   2.   Douglas, T.A. *et al.* The fate of mercury in Arctic terrestrial and aquatic ecosystems, a review.
368   *Environ. Chem.* **9**, 321 (2012).
369   3.   AMAP, "AMAP Assessment 2011: Mercury in the Arctic. Arctic Monitoring and Assessment
370   Programme (AMAP)" (Oslo, Norway, 2011).
371   4.   Dietz, R. *et al.* Time trends of mercury in feathers of West Greenland birds of prey during 1851-
372   2003. *Environ. Sci. Techn*. **40**, 5911 (2006).
373   5.   Dietz, R. *et al.* Trend in mercury in hair of Greenlandic polar bears (Ursus maritiumus) during 1892-
374   2001. *Environ. Sci. Techn*. **40**, 1120 (2006).
375   6.   Outridge, P.M. *et al*. A comparison of modern and pre-industrial levels of mercury in the teeth of
376   *Beluga* in the Mackenyie Delta, Northwest Territories, and *Walrus* at Iglookik, Nunavut, Canada.
377   *Arctic*, **55**, 123 (2002).
378   7.   Johnson, K. P. *et al.* Investigation of the deposition and emission of mercury in arctic snow during
379   an atmospheric mercury depletion event. *J. Geophys. Res.* **113**, D17, D17304 (2008).
380   8.   NADP 2016. National Atmospheric Depostion Program, Annual Data, all MDN sites.
381   http://nadp.sws.uiuc.edu/data/mdn/annual.aspx (Oct 3, 2016).
382   9.   Schuster P. F. *et al.* Mercury export from the Yukon river basin and potential response to a
383   changing climate. *Environ. Sci. Technol.* **45**, 9262-9267 (2011).

384 10.   Fisher J. A. *et al.* Riverine source of Arctic Ocean mercury inferred from atmospheric observations.
385   *Nat. Geosci.* **5**, 499-504 (2012).
386 11.   Dastoor, A. P. & Durnford, D. A. Arctic Ocean: Is It a sink or a source of atmospheric mercury?
387   *Environ. Sci. Technol.* **48**, 1707-1717 (2014).
388 12.   Demers, J. D., Blum, J.D. & Zak, D. R. Mercury isotopes in a forested ecosystem: Implications for
389   air-surface exchange dynamics and the global mercury cycle. *Global Biogeochem Cy.* **27**, 222-238
390   (2013).
391 13.   Jiskra, M. *et al.* Mercury deposition and re-emission pathways in boreal forest soils investigated
392   with Hg isotope signatures. *Environ. Sci. Technol.* **49**, 7188-7196 (2015).
393 14.   Enrico, M. *et al.* Atmospheric mercury transfer to peat bogs dominated by gaseous elemental
394   mercury dry deposition. *Environ. Sci. Technol.* **50**, 2405-2412 (2016).
395 15.   Zheng, W., Obrist, D., Weis, D., & Bergquist, B. A. Mercury isotope compositions across North
396   American forests. *Global Biogeochem Cy.* **30**, 1475-1492 (2016).
397 16.   Krabbenhoft, D. & Sunderland, E.M. Global Change and Mercury. *Science* **341**, 1457-1458 (2013).
398 17.   Polyakov IV, Alekseev GV, Bekryaev RV, Bhatt U, Colony RL, Johnson MA, et al. Observationally
399   based assessment of polar amplification of global warming. *Geophys. Res. Letters* **29**, 1878 (2002).
400 18.   ACIA, "Impacts of a warming Arctic: Arctic Climate Impact Assessment. ACIA Overview report"
401   (Cambridge University Press, 2004).
402 19.   Selin N.E, Global change and mercury cycling: challenges for implementing a global treaty.
403   *Environmental Toxicology and Chemistry* **33**, 1202 (2014).
404 20.   Smith-Downey, N. V., Sunderland, E. M. & Jacob, D. J. Anthropogenic impacts on global storage
405   and emissions of mercury from terrestrial soils: Insights from a new global model. *J Geophys Res-
406   Biogeo.* **115**, 11 (2010).
407 21.   Steffen, A. *et al.* A synthesis of atmospheric mercury depletion event chemistry in the atmosphere
408   and snow. *Atmos. Chem. Phys.* **8**, 1445-1482 (2008).
409 22.   Agnan, Y. *et al*. New constraints on terrestrial surface-atmosphere fuxes of gaseous elemental
410   mercury using a global database. *Environ. Sci. Technol.* **50**, 507-524 (2016).
411 23.   Sherman L. S. *et al.* Mass-independent fractionation of mercury isotopes in Arctic snow driven by
412   sunlight. *Nat. Geosci.* **3**, 173-177 (2010).
413 24.   Biswas, A. *et al.* Natural mercury isotope variation in coal deposits and organic soils. *Environ. Sci.
414   Technol.* **42**, 8303-8309 (2008).
415 25.   Obrist, D., Pokharel, A. K. & Moore, C. Vertical profile measurements of soil air suggest
416   immobilization of gaseous elemental mercury in mineral soil. *Environ. Sci. Technol.* **48**, 2242-2252
417   (2014).
418 26.   Obrist et al. Mercury distribution across 14 U.S. Forests. Part I: spatial patterns of concentrations
419   in biomass, litter, and soils. *Environ. Sci. Technol.* 45, 3974-3981 (2011).
420 27.   Smith D.B. et al. Geochemical and mineralogical data for soils of the coterminous United States.
421   *U.S. Geological Survey Data Series* **801**, 386p (2013).
422 28.   Amos H. M. *et al.* Observational and modeling constraints on global anthropogenic enrichment of
423   mercury. *Environ. Sci. Technol.* **49**, 4036-4047 (2015).
424 29.   Hararuk, O., Obrist, D. & Luo, Y. Modelling the sensitivity of soil mercury storage to climate-
425   induced changes in soil carbon pools. *Biogeosciences* **10**, 2393-2407 (2013).
426 30.   Sprovieri F, *et al*. Atmospheric mercury concentrations observed at ground-based monitoring sites
427   globally distributed in the framework of the GMOS network. *Atmos. Chem Phys.* **16**, 11915-11935.
428   (2016).
429

430 **Methods References**

431   31.   Fritsche, J. *et al.* Elemental mercury fluxes over a sub-alpine grassland determined with two
432   micrometeorological methods. *Atmos. Environ.* **42**, 2922-2933 (2008).
433   32.   Castro, M. & Moore, C. Importance of gaseous elemental mercury fluxes in western Maryland.
434   *Atmosphere* **7**, 110 (2016).
435   33.   Douglas, T. A. *et al.* Influence of snow and ice crystal formation and accumulation on mercury
436   deposition to the Arctic. *Environ. Sci. Technol.* **42**, 1542-1551 (2008).
437   34.   Cole, A.S. *et al.* Ten-year trands of atmospheric mercury in the high Arctic compared to Canadian
438   sub-Arctic and mid-latitude sites. *Atmsph. Chem. Phys.* **13**, 1535 (2013).
439   35.   Seok, B. *et al.* An automated system for continuous measurements of trace gas fluxes through
440   snow: an evaluation of the gas diffusion method at a subalpine forest site, Niwot Ridge, Colorado.
441   *Biogeochemistry* **95**, 95-113 (2009).
442   36.   Faïn, X. *et al*. Mercury dynamics in the Rocky Mountain, Colorado, snowpack. *Biogeosciences* **10**,
443   3793-3807 (2013).
444   37.   Moore, C. W., Obrist, D. & Luria, M. Atmospheric mercury depletion events at the Dead Sea:
445   Spatial and temporal aspects. *Atmos. Environ.* **69**, 231-239 (2013).
446   38.   Edwards, G. C. *et al.* Development and evaluation of a sampling system to determine gaseous
447   mercury fluxes using an aerodynamic micrometeorological gradient method. *J. Geophy. Res.-*
448   *Atmos.* **110**, (2005).
449   39.   Lyman, S. N. & Jaffe, D. A. Formation and fate of oxidized mercury in the upper troposphere and
450   lower stratosphere. *Nat Geosci* **5**, 114-117 (2012).
451   40.   Zhang, L., Wright, L. P. & Blanchard, P. A review of current knowledge concerning dry deposition
452   of atmospheric mercury. *Atmos. Environ.* **43**, 5853-5864 (2009).
453   41.   Shaver, G. R., Chapin, F. S. Production: Biomass relationships and element cycling in contrasting
454   Arctic vegetation types. *Ecol. Monogr.* **61**, 1-31 (1991).
455   42.   Chapin, F. S., Shaver, G. R., Giblin, A. E., Nadelhoffer, K. J. & Laundre, J. A. Responses of Arctic
456   tundra to experimental and observed changes in climate. *Ecology* **76**, 694-711 (1995).
457   43.   Fu, X. , Heimburger, L.-E. & Sonke, J. E. Collection of atmospheric gaseous mercury for stable
458   isotope analysis using iodine- and chlorine-impregnated activated carbon traps. *J. Anal. At.*
459   *Spectrom.* **29**, 841-852 (2014).

460
461

470

471   **Author contributions:** D.O. and D.H. designed and initiated the project, and M.J., J.S. and D.O.
472   designed and developed the isotope component. All authors were involved in all major field
473   sampling and/or laboratory analyses. Y.A. led data analysis and M.J. led stable isotope sampling
474   and analysis with support by J.S. D.O. led manuscript writing with major support by M.J. Y.A.
475   J.S. and C.M.

476   **Additional information:** Supplementary Information accompanies this paper at
477   http://www.nature.com/

478   **Competing financial interests:** The authors declare no competing financial interests.

479   **Data availability statement:** Hg Concentration data in plants, soils, precipitation and snowpack
480   generated during this study are included in the Extended Data section as Tables. Stable isotope
481   data are also included in Extended Data and in Supplementary Information. Additional data (e.g.,
482   flux data) as well as higher-resolution datasets are available from the corresponding author on
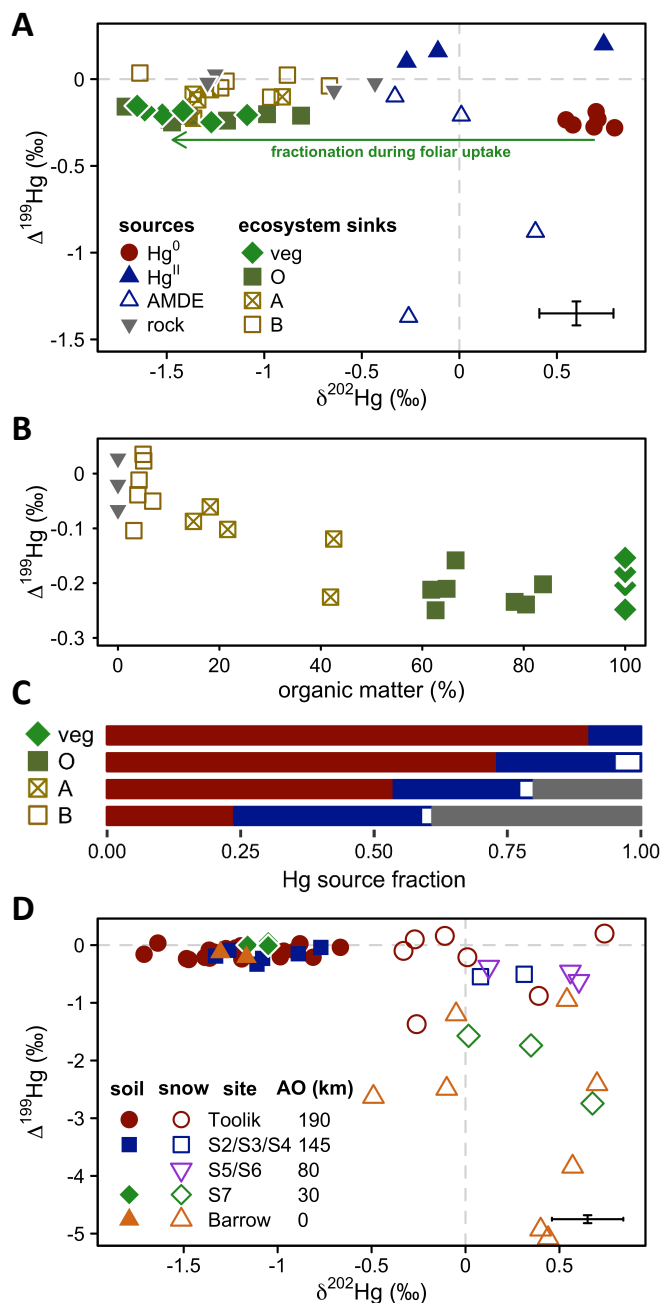483   reasonable request.

484
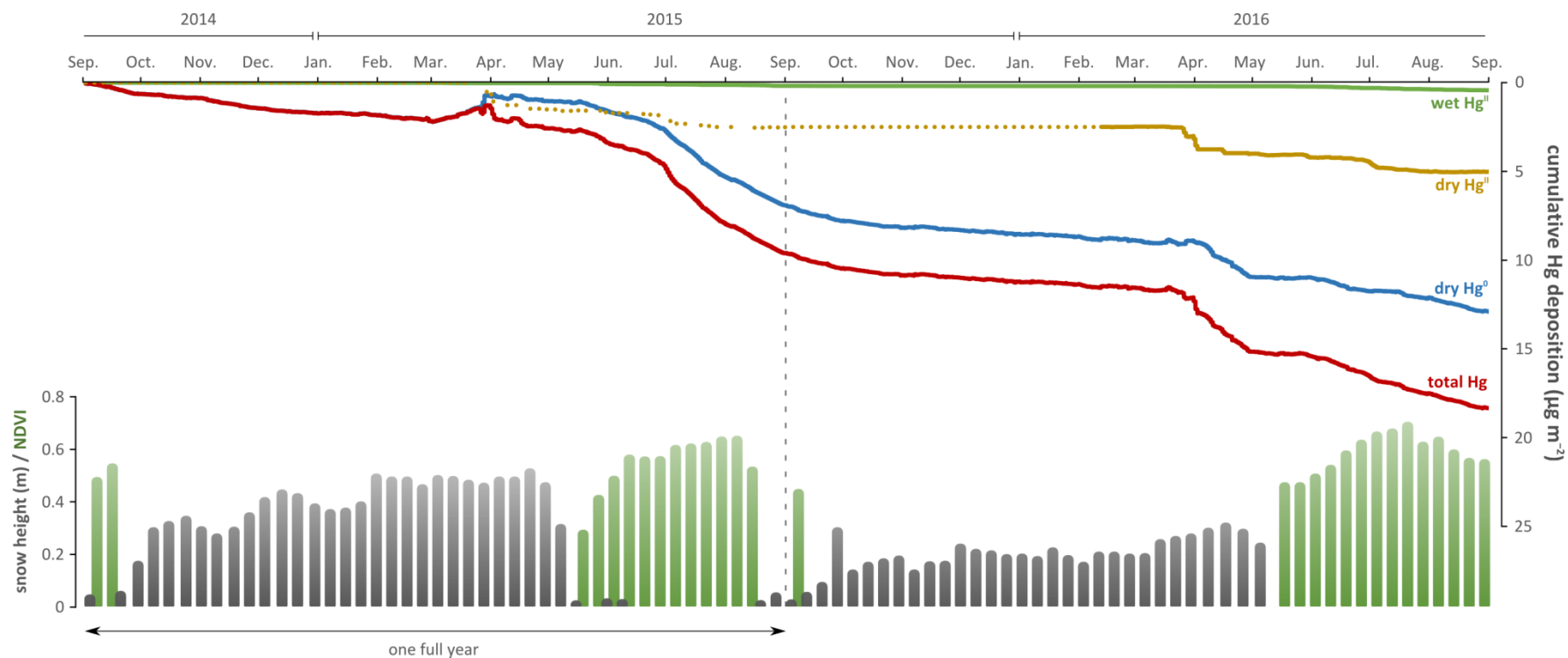
Figure 1. Cumulative atmospheric deposition of major Hg forms in the Arctic tundra. Blue line: gaseous Hg^0 flux; green line: wet Hg deposition (Hg^{II}) ; brown line: dry deposition of Hg^{II}; dashed line shows observations extrapolated when not measured. Bottom panel shows snow heights and vegetation coverage.

485

Figure 2 A. Mass-dependent (δ^{202}Hg) and mass-independent (Δ^{199}Hg) mercury isotope signatures in the tundra. Uncertainty (2 SD of replicate standards) shown on lower right. Symbols for sources include: filled circles for atmospheric Hg^0; filled triangles for Hg^{II} in snow deposited before Jan/Feb 2016; open triangles for Hg^{II} measured in surface snow during periods of AMDEs (Mar/Apr 2016); and filled inverted triangles for geogenic Hg in rock samples. Symbols for tundra samples include: filled diamonds for bulk vegetation; filled squares for organic (O-horizon) soils; and open squares for mineral soils (with cross for A horizons [>10% organic matter] and without cross for B horizons [<10% organic matter]). Arrow represents mass-dependent fractionation of atmospheric Hg^0 during foliar uptake. **B. Linear correlation of Δ^{199}Hg with organic matter content**, showing that signatures of terrestrial samples can be explained predominantly by binary mixing of the two endmembers geogenic Hg and vegetation Hg. **C. Fraction of respective Hg sources in vegetation and soils. D. δ^{202}Hg and Δ^{199}Hg mercury isotope signatures of soils (O, A, B horizons) and snow (collected during Mar/Apr)** along an inland-to-coastal transect. Distance from Arctic Ocean (AO) is given in km. Barrow samples are from [23,24].

486
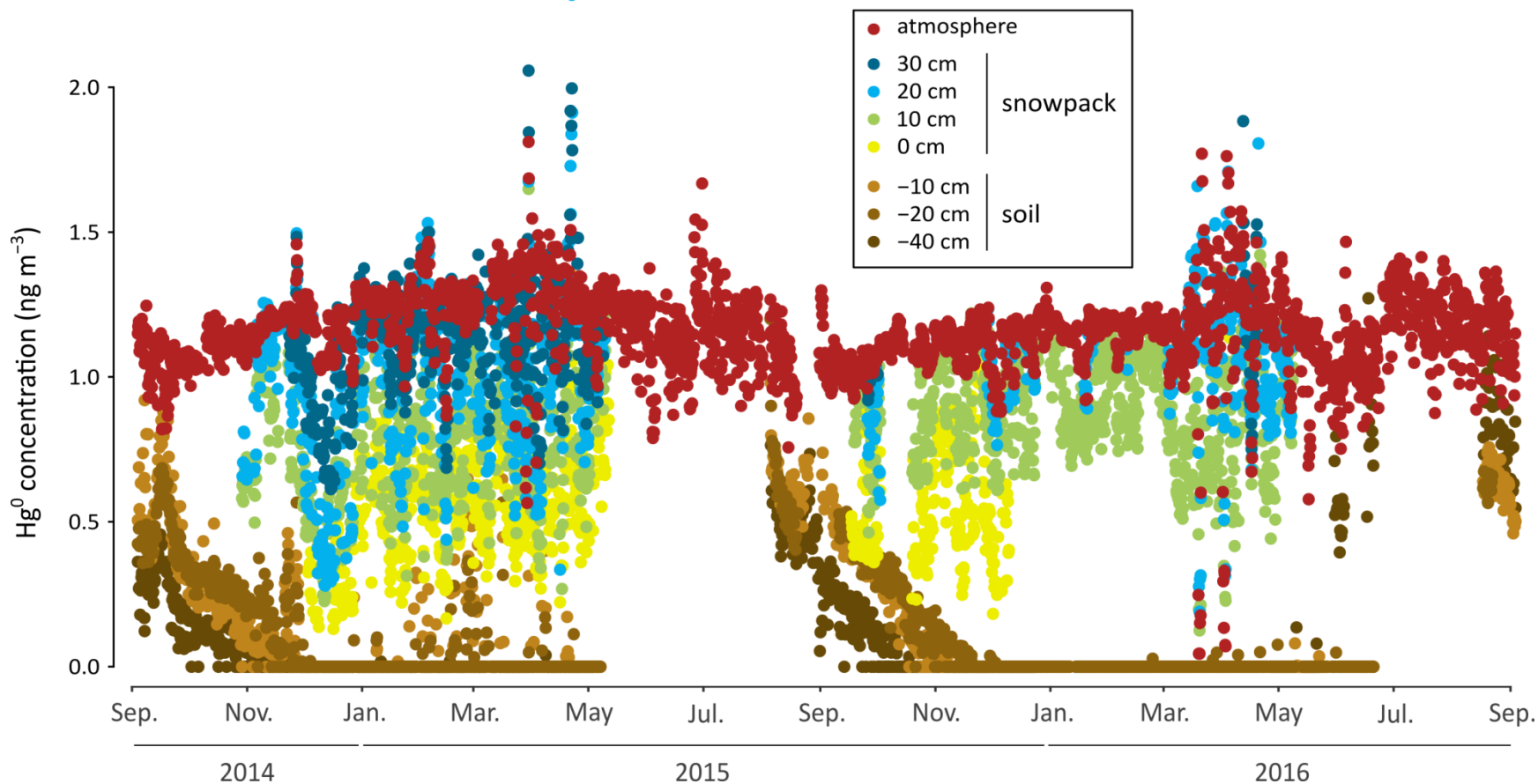
Figure 3. Gaseous Hg[0] concentrations in the atmosphere, interstitial snow air, and tundra soil pores. Zero-values in soils show concentration measurements below the detection limits. Different symbol colors represent different heights in snowpack and different depths in soils. Snowpack heights (in cm) show height in snowpack above the ground surface. Soil depth (in cm, negative numbers) show depth of measurements in soil pores below the ground surface.